Cell Metabolism
Article

S6 Kinase Deletion Suppresses Muscle Growth Adaptations to Nutrient Availability by Activating AMP Kinase

Victor Aguilar,[1,2,12] Samira Alliouachene,[1,2,12] Athanassia Sotiropoulos,[1,2,12] Andrew Sobering,[1,2] Yoni Athea,[3,4] Fatima Djouadi,[5] Sylvain Miraux,[6] Eric Thiaudière,[6] Marc Foretz,[7,8] Benoit Viollet,[7,8] Philippe Diolez,[6] Jean Bastin,[5] Paule Benit,[9] Pierre Rustin,[9] David Carling,[10] Marco Sandri,[11] Renée Ventura-Clapier,[3,4] and Mario Pende[1,2,*]

[1] INSERM, U845, Paris F-75015, France
[2] Université Paris Descartes, UMRS-845, Paris F-75015, France
[3] INSERM, U769, Châtenay-Malabry F-92296, France
[4] Université Paris-Sud, Faculté de Pharmacie, IFR141, Châtenay-Malabry F-92296, France
[5] CNRS, UPR 9078, Université Paris Descartes, Paris F-75015, France
[6] CNRS, UMR 5536, Bordeaux F-33076, France
[7] INSERM, U567, Paris F-75014
[8] Institut Cochin, Université Paris Descartes, CNRS, UMR 8104, Paris F-75014, France
[9] INSERM, U676, Paris F-75019, France
[10] Cellular Stress Group, MRC Clinical Sciences Centre, Imperial College, Hammersmith Hospital, London W12 0NN, UK
[11] Dulbecco Telethon Institute at the Venetian Institute of Molecular Medicine, Department of Biomedical Science, University of Padova, Padova 35129, Italy
[12] These authors contributed equally to this work.
*Correspondence: pende@necker.fr
DOI 10.1016/j.cmet.2007.05.006

SUMMARY

S6 kinase (*S6K*) deletion in metazoans causes small cell size, insulin hypersensitivity, and metabolic adaptations; however, the underlying molecular mechanisms are unclear. Here we show that *S6K*-deficient skeletal muscle cells have increased AMP and inorganic phosphate levels relative to ATP and phosphocreatine, causing AMP-activated protein kinase (AMPK) upregulation. Energy stress and muscle cell atrophy are specifically triggered by the *S6K1* deletion, independent of S6K2 activity. Two known AMPK-dependent functions, mitochondrial biogenesis and fatty acid β-oxidation, are upregulated in *S6K*-deficient muscle cells, leading to a sharp depletion of lipid content, while glycogen stores are spared. Strikingly, AMPK inhibition in *S6K*-deficient cells restores cell growth and sensitivity to nutrient signals. These data indicate that S6K1 controls the energy state of the cell and the AMPK-dependent metabolic program, providing a mechanism for cell mass accumulation under high-calorie diet.

INTRODUCTION

In mammals, S6 kinases 1 and 2 (S6K1/2) are serine/threonine kinases that transduce the anabolic signals from nutrition (Um et al., 2006). Insulin, insulin-like growth factor (IGF) peptides, glucose, and amino acids initiate intracellular pathways that converge on the activation of the mammalian target of rapamycin (mTOR) complex, a key event in the regulation of S6K (Sarbassov et al., 2005). Growth-factor peptides control mTOR/S6K via class 1a phosphatidylinositol 3-kinase (PI3K), Akt kinases, the tuberous sclerosis complex proteins 1 and 2 (TSC1/2), and the small GTPase Rheb, while nutrients require class 3 PI3K (Nobukuni et al., 2005). In addition, nutrient availability indirectly controls mTOR/S6K by altering the energy status of the cell. High ATP levels increase the catalytic activity of mTOR (Dennis et al., 2001), while the AMP/ATP ratio modulates AMP-activated protein kinase (AMPK). In turn, AMPK controls the activity of TSC2 and inhibits mTOR signaling (Krause et al., 2002; Inoki et al., 2003).

That S6K is involved in sensing nutrient availability and mediating growth responses is suggested by the phenotype of *S6K* mutant animals. *S6K* null flies are developmentally delayed and small due to a reduction of cell size (Montagne et al., 1999). Similarly, *S6K1*-deficient mice have an approximately 20% reduction in body weight as compared to wild-type mice (Shima et al., 1998). The growth defect is more pronounced in nutrient- and insulin/IGF-target tissues such as pancreatic β cells, skeletal muscle, and adipose tissue, where the size of mutant cells is sharply reduced (Pende et al., 2000; Um et al., 2004; Ohanna et al., 2005). In many regards, the *S6K1* deletion mimics the metabolic adaptations to a low-calorie diet. Glucose-stimulated insulin secretion and blood insulin levels are low in these mice (Pende et al., 2000), while lipolysis is increased (Um et al., 2004). In addition,

S6K$^{-/-}$ skeletal muscle mass is refractory to starvation and is equivalent to starved wild-type mice (Ohanna et al., 2005). Finally, on a high-fat diet, *S6K1*-deficient mice do not become obese (Um et al., 2004).

How S6K1 exerts its anabolic action is unclear. One possibility is that it upregulates protein synthesis by phosphorylating ribosomal protein S6 (rpS6), initiation factor eIF4B, elongation factor 2 kinase (eEF2K), or other substrates involved in translational control (Sarbassov et al., 2005). Consistent with this possibility, S6K1 associates with a translation preinitiation complex in a growth-factor- and nutrient-dependent manner (Holz et al., 2005). However, S6K2 can rescue rpS6 phosphorylation but cannot compensate for the growth defect due to *S6K1* deletion, indicating that ribosomal phosphorylation does not correlate with the growth state of the cell (Ohanna et al., 2005). Moreover, the combined deletion of *S6K1* and *S6K2* (*S6K1;S6K2*$^{-/-}$) in fibroblasts and embryonic stem cells does not affect global translation initiation, as assessed by the polysome/monosome ratio, or the translation of specific classes of mRNAs under the control of the mTOR pathway, such as the 5′-terminal oligopyrimidine tract (5′TOP) mRNAs (Pende et al., 2004). Thus, the molecular changes underlying the growth defects and metabolic adaptations of *S6K*-deficient tissues remain unclear.

Since growth requires ATP, growth-factor pathways have evolved molecular mechanisms to upregulate the energy status of the cell (Hammerman et al., 2004). Particularly, the Akt kinases have pleiotropic effects on nutrient uptake, glycolysis, and oxidative phosphorylation (Edinger and Thompson, 2002; Majewski et al., 2004), leading to increased high-energy phosphate levels that may activate the mTOR/S6K pathway (Hahn-Windgassen et al., 2005). Here we address whether the *S6K* deletion affects energy production. We find that *S6K1;S6K2*$^{-/-}$ muscles have an increased AMP/ATP ratio, causing AMPK activation. This response is also observed in other tissues and depends on S6K1 activity. Finally, we provide evidence that the AMPK activation contributes to the atrophic adaptations of *S6K1*-deficient mice. We conclude that the growth-regulating mTOR/S6K1 kinases control an AMPK-dependent metabolic program.

RESULTS

Energy Stress in *S6K*-Deficient Mice

The deletion of *S6K1* and *S6K2* caused an ~20% reduction of muscle cell diameter at the myotube stage (Figure 1A; Ohanna et al., 2005). To address whether a defect in energy production affects the size of cultured muscle cells, wild-type and *S6K1;S6K2*$^{-/-}$ cells were treated with oligomycin and 2-deoxyglucose, which inhibit mitochondrial ATP synthase and glycolysis, respectively. Wild-type cell size was significantly reduced by both energy-depriving agents (Figure 1A). Conversely, *S6K* mutant cells displayed a partial resistance. Moreover, energy-deprived wild-type cells were comparable in size to *S6K*-deficient cells. Thus, energy deprivation and *S6K* deletion affect muscle cell size through mechanisms that might be partly shared.

To evaluate whether the *S6K* deletion alters the energy state of skeletal muscle cells, we first assayed the adenine nucleotide pools and phosphocreatine (PCr) in skeletal muscle by enzymatic reactions. Strikingly, AMP levels were increased by 40% in *S6K1;S6K2*$^{-/-}$ muscles, while total ATP levels did not differ from the control, leading to a higher AMP/ATP ratio in mutant muscles. (Figure 1B). Since the ATP concentration in skeletal muscle is kept relatively constant by the creatine kinase reaction, we asked whether a drop in phosphocreatine levels accompanied the rise in AMP levels of *S6K* null muscles. Although a statistically significant difference was not reached, there was a tendency toward a reduction of the PCr pool relative to the ATP pool in mutant muscles (Figure 1B). To confirm these data, ^{31}P NMR quantitation of phosphorus metabolites was performed in the gastrocnemius muscles of live mice at rest. The AMP concentration was below detection level by ^{31}P NMR spectroscopy, though the 30% increase in inorganic free phosphate (Pi) of *S6K*-deficient muscles was consistent with mutant mice presenting a depletion of high-energy phosphates (Figure 1C). Strikingly, the Pi increase in *S6K* mutant muscles was accompanied by an equivalent decrease of PCr levels. The mean values of the phosphorus metabolites allowed an estimation of the fall in the cytosolic free energy of ATP hydrolysis (ΔGp) in the *S6K* mutant muscles (Figure 1C). In conclusion, the combined deletion of *S6K1* and *S6K2* causes a dissipation of available free energy in skeletal muscles.

To determine the adenine nucleotide levels in tissue lacking the creatine/PCr system, we assayed ATP in livers from mutant mice. As shown in Figure S1 in the Supplemental Data available with this article online, ATP levels were reduced by 34% in *S6K1;S6K2*$^{-/-}$ livers. Thus, *S6K* deficiency causes a depletion of energy supplies in the form of PCr in skeletal muscles and in the form of ATP in other tissues such as liver.

Despite their high homology, S6K1 and S6K2 differ in their ability to promote muscle cell growth and sensitivity to environmental cues, as these responses depend on S6K1 activity (Pende et al., 2000; Um et al., 2004; Ohanna et al., 2005). Thus, we determined which gene deletion triggered a state of energy deprivation in muscle. The deletion of *S6K1* was sufficient to increase the AMP/ATP ratio, while the *S6K2*-deficient muscles did not differ as compared to the wild-type (Figure 1D). Taken together, these data indicate that the atrophic state of the *S6K* mutant mice correlates with a decrease in high-energy phosphate levels.

S6K Deletion Sensitizes Cells to AMPK Action

The concentration of adenine nucleotides tightly regulates the balance between anabolic and catabolic processes (Atkinson, 1970), in part through the activation of AMPK during energy stress and increased AMP/ATP ratio (Kahn et al., 2005). The heterotrimeric AMPK complex, consisting of a catalytic subunit (α) and two regulatory subunits (β and γ), has multiple substrates that are

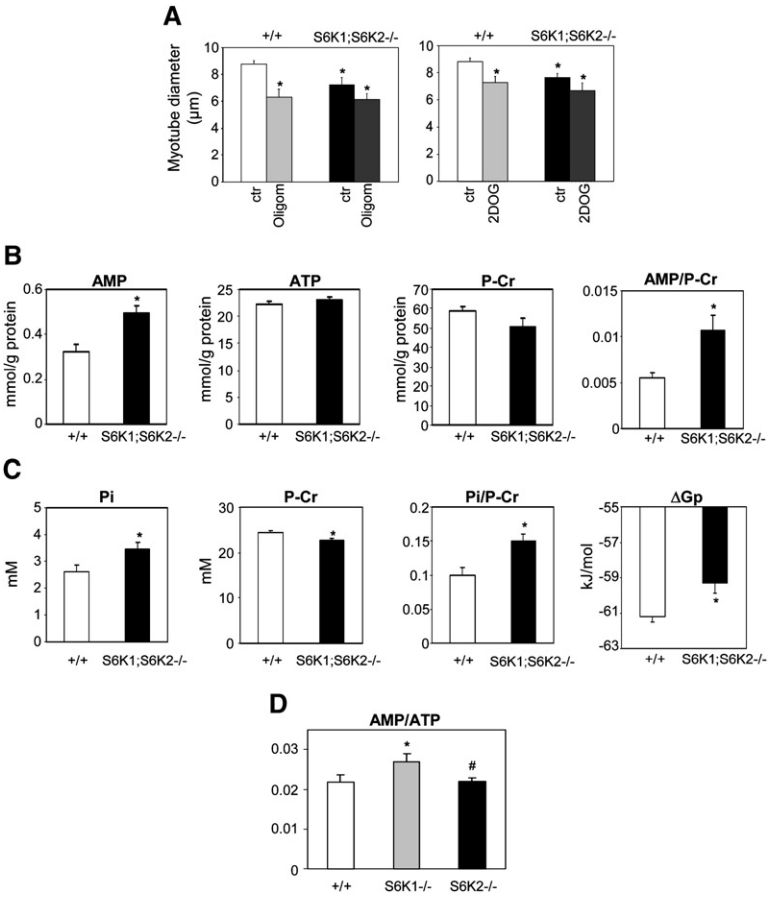

Figure 1. Energy Stress in *S6K1*-Deficient Skeletal Muscles

(A) Cells were allowed to differentiate for 2 days in 2% horse serum and then incubated for 2 days in the presence or absence of 20 nM oligomycin (Oligom) or 20 mM 2-deoxyglucose (2DOG). Myotube diameter was measured at day 4 of differentiation. Histograms show results for at least three assays. Independent cell cultures were obtained from at least two mice of the indicated genotype. *p < 0.05 versus wild-type control. Oligomycin- or 2DOG-treated *S6K1;S6K2*$^{-/-}$ cells were not significantly different from untreated mutant cells. In this and all other figures, error bars represent ±SEM.

(B) Metabolites were extracted from hindlimb muscles of the indicated genotype. Histograms are means from at least four mice. *p < 0.05 versus wild-type genotype.

(C) In vivo energy phosphate levels were assessed in hindlimb muscles by ^{31}P NMR. n ≥ 8 mice. *p < 0.05 versus wild-type genotype.

(D) Energy phosphate levels were assessed by enzymatic procedure as in (B). *p < 0.05 versus wild-type genotype; #p < 0.05 versus *S6K1* genotype.

involved in reprogramming sugar, fat, and protein metabolism. Since *S6K*-deficient muscles had a higher AMP/ATP ratio, we evaluated AMPK activity in these cells by immunoblot analysis against phospho-Thr172 AMPKα. Of note, the basal phosphorylation of AMPK was approximately 3-fold higher in *S6K*-deficient myotube cultures as compared to wild-type (Figures 2A and 2B). In addition, AMPK phosphorylation in mutant muscle cells displayed higher sensitivity to increasing doses of oligomycin (Figure 2A). Thus, the shutdown of the S6K pathway in muscle cells upregulates AMPK activity. Importantly, AMPK activation is observed in a pure population of *S6K*-deficient muscle cells, suggesting that this regulation does not involve humoral factors and is a likely consequence of increased intracellular AMP concentration, the allosteric regulator of AMPK.

To evaluate the functional consequence of AMPK activation, we assessed the phosphorylation of the AMPK substrate acetyl-CoA carboxylase (ACC), the enzyme that catalyzes the conversion of acetyl-CoA to malonyl-CoA in the cytosol (Kahn et al., 2005). Malonyl-CoA is an intermediate in fatty acid synthesis and an allosteric inhibitor of carnitine palmitoyltransferase 1, which regulates the transfer of long-chain acyl-CoAs from the cytosol into the mitochondria. The AMPK-mediated phosphorylation of ACC decreases enzyme activity, resulting in increased oxidation of long-chain acyl-CoAs. ACC phosphorylation was stimulated in *S6K1;S6K2*$^{-/-}$ cells, consistent with the AMPK upregulation (Figure 2C, lanes 1 and 2). In addition, *S6K1;S6K2*$^{-/-}$ myotubes displayed a sharp reduction of total ACC levels similar to that observed in cells expressing a constitutively active *AMPK* allele (Foretz et al., 2005). Thus, in *S6K1;S6K2*$^{-/-}$ myotubes, the relative amount of active unphosphorylated ACC is decreased due to the coordinated effect on AMPK-mediated ACC phosphorylation and expression.

AMPK is the molecular target of the antidiabetic drug metformin, which improves glucose homeostasis and insulin sensitivity (Kahn et al., 2005). A 2 day treatment of wild-type myotubes with metformin increased AMPK activity while reducing S6K and 4EBP-1 phosphorylation, consistent with the reported action of AMPK on TSC2 (Figure 2D). However, the inhibition of the mTOR pathway by metformin was partial, as indicated by the residual phosphorylation of both mTOR substrates and of rpS6. Conversely, the macrolide rapamycin sharply inhibited mTORC1 signaling, as judged by the absence of detectable S6K and rpS6 phosphorylation. In addition this long-term incubation of myotubes with rapamycin also decreased the phosphorylation of the mTORC2 substrate Akt, possibly as a consequence of reduced mTORC2 complex formation (Sarbassov et al., 2006). mTOR downregulation by rapamycin was sufficient to increase the AMP/ATP ratio by 87% in cultured myotubes (AMP/ATP

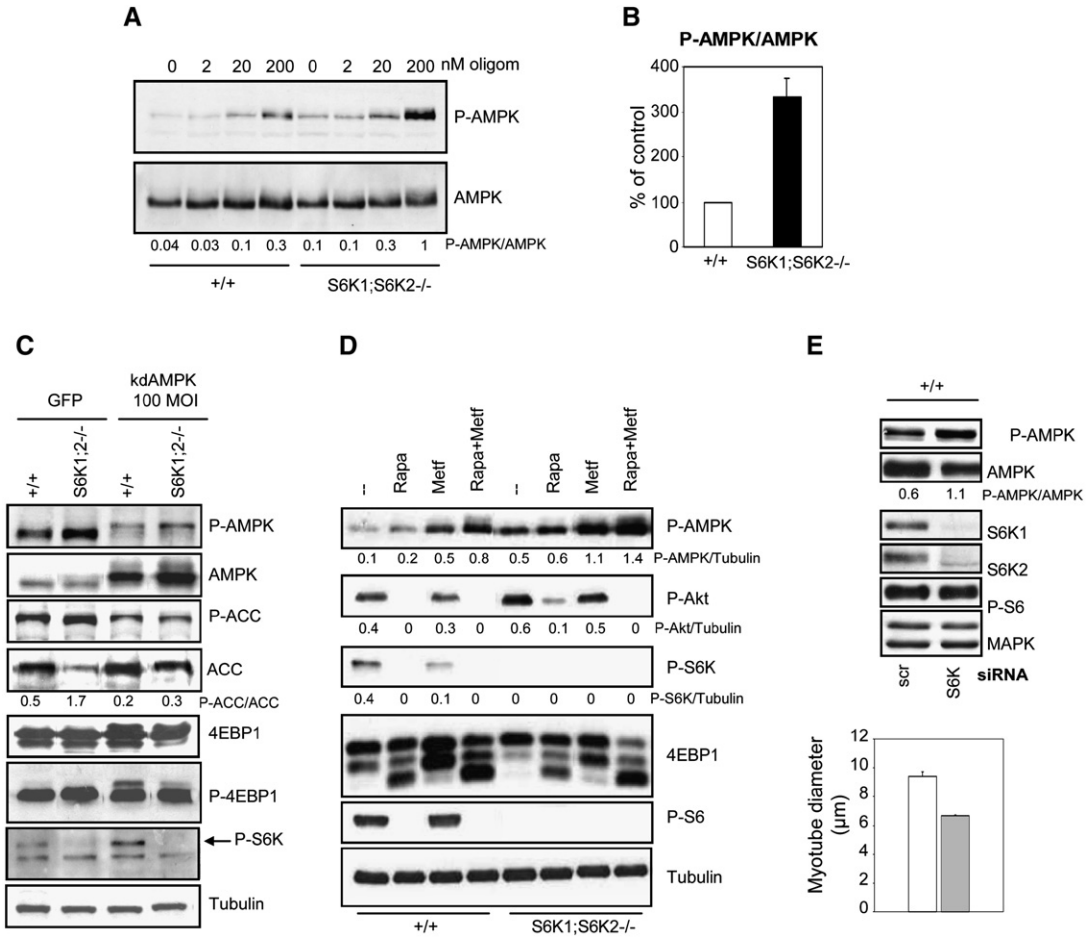

Figure 2. AMPK Activation in *S6K*-Deficient Muscle Cells

(A) Immunoblot analysis of protein extracts from myotubes of the indicated genotype using anti-phospho-Thr172 AMPKα and anti-AMPKα antibodies. Cells were allowed to differentiate for 4 days and were treated for 30 min with oligomycin (2 to 200 nM). Ratio of phospho-AMPKα to total AMPKα signal intensity is indicated.

(B) Average of phospho-AMPKα to total AMPKα ratios from three distinct cultures in basal conditions.

(C and D) Immunoblot analysis of protein extracts from myotubes using the indicated antibodies. Muscle cells were allowed to differentiate for 2 days and were transduced with *GFP* or *kd-AMPK* adenoviruses at the indicated moi (C) or were treated with 0.25 mM metformin or 20 nM rapamycin (D). Cell lysates were prepared 2 days later.

(E) Immunoblot analysis of protein extracts from myotubes using the indicated antibodies. Cells were transfected with 20 nM control or *S6K* siRNA at day 1 of differentiation and harvested 3 days later. The lower panel shows the average myotube diameter from three distinct experiments.

ratio of 0.08 ± 0.01 in untreated myotube cells at day 4 of differentiation and 0.15 ± 0.02 after a 2 day treatment with rapamycin). Interestingly, the combination of rapamycin and metformin cooperated in stimulating AMPK phosphorylation, suggesting that mTOR inhibition can potentiate metformin action on AMPK. Similarly, the stimulatory effect of metformin on AMPK was more pronounced in *S6K1;S6K2*$^{-/-}$ myotubes, suggesting that the complete inactivation of *S6K* genes sensitizes the cells to the AMPK-activating agents. As previously reported (Um et al., 2004), *S6K1;S6K2*$^{-/-}$ cells also presented an upregulation of Akt activity (Figure 2D). Thus, *S6K* deletion ameliorates both AMPK and Akt signaling, two major pathways in the control of nutrient homeostasis.

To address whether a transient inactivation of S6K signaling is sufficient to upregulate the AMPK pathway in muscle cells, wild-type myotube cultures were transfected with small interfering RNA (siRNA) targeting both *S6K1* and *S6K2* mRNAs. Although the siRNA effectively reduced S6K expression, the impact on rpS6 phosphorylation was minor, possibly due to residual kinase activity (Figure 2E). However, this decrease in S6K expression was sufficient to upregulate AMPK activity and concomitantly affect cell growth. Thus, the effects on AMPK activity and cell size are early events after the shutdown of S6K signaling.

Next we addressed which *S6K* gene affects AMPK signaling. Consistent with the effect on AMP levels (Figure 1D), *S6K1* deletion was sufficient to increase AMPK phosphorylation to the same extent as the combined deletion of *S6K1* and *S6K2* genes (Figure S2). Importantly, this effect correlated with myotube atrophy.

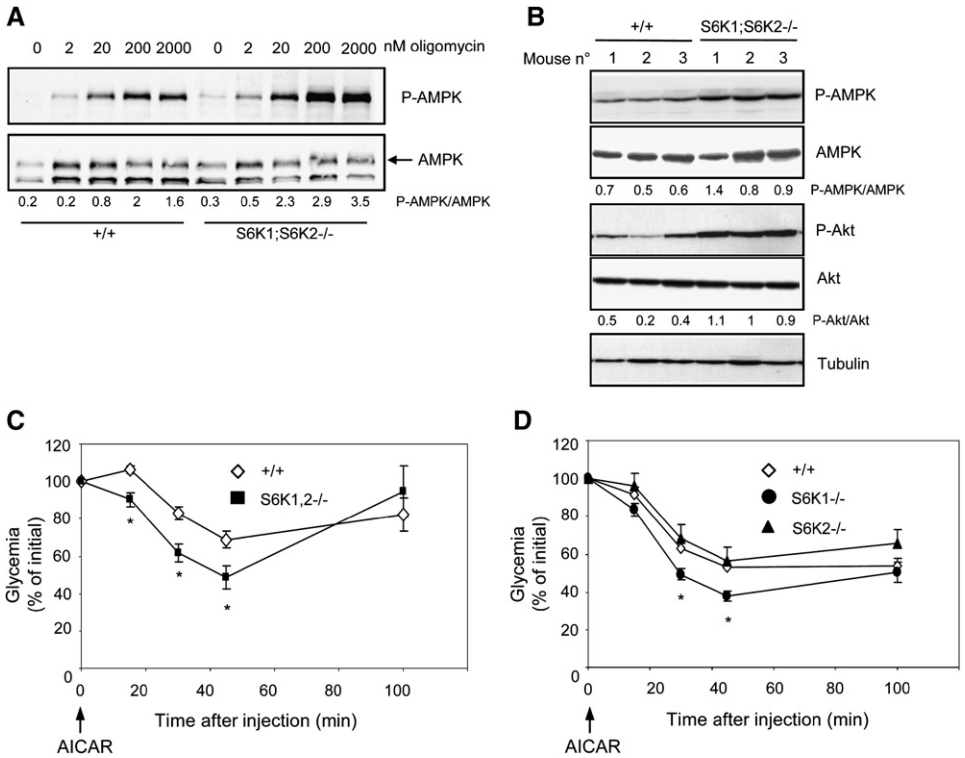

Figure 3. Whole-Body Increased Sensitivity to AMPK Activation in *S6K*-Deficient Mice

(A and B) Immunoblot analysis of protein extracts from hepatocytes (A) or adipose tissue (B) of the indicated genotype using anti-phospho-Thr172 AMPKα and anti-AMPKα antibodies. Hepatocytes were treated for 30 min with oligomycin (2 to 2000 nM). Epididymal fat pads from three different mice for each genotype were analyzed.

(C and D) AICAR tolerance test was performed by intraperitoneal injection of 0.15 g AICAR per kg body weight into overnight-fasted 5-month-old mice. Basal glucose levels for wild-type and *S6K1;S6K2*$^{-/-}$ mice were 80.7 ± 3.4 and 72.7 ± 3.9 mg/dl, respectively (C). Basal glucose levels for wild-type, *S6K1*$^{-/-}$, and *S6K2*$^{-/-}$ mice were 111.8 ± 6.7, 109.5 ± 4.7, and 107.8 ± 9.4 mg/dl, respectively (D). n = 6–15; *p < 0.05 versus wild-type group.

To determine whether AMPK control by S6K is specific to muscle cells, we extended our analysis to liver and fat tissues. As shown in Figure 3A, primary hepatocytes from *S6K*-deficient mice also had higher basal and oligomycin-induced AMPK activation as compared to wild-type. Similarly, *S6K1;S6K2*$^{-/-}$ epididymal fat pads from randomly fed mice displayed increased phosphorylation of AMPK (Figure 3B). In addition, *S6K*-deficient fat tissues presented higher levels of Akt phosphorylation. Thus, the deletion of *S6K* causes a general activation of the AMPK pathway in multiple tissues, and in a cell-autonomous manner. Of note, this effect is concomitant with an upregulation of the insulin/Akt anabolic pathway.

To evaluate whether the *S6K* deletion is sufficient to affect AMPK-dependent whole-body glucose homeostasis, blood glucose was assayed after an intraperitoneal injection of the cell-permeable AMPK activator 5-aminoimidazole-4-carboxamide ribonucleoside (AICAR). As shown in Figure 3C, AICAR caused a 30% reduction in blood glucose levels of wild-type mice, possibly due to the combined effects on muscle glucose uptake activation and hepatic glucose output inhibition (Mu et al., 2001). Strikingly, the hypoglycemic effect of AICAR was more pronounced in *S6K1;S6K2*$^{-/-}$ mice. In addition, the single deletion of *S6K1* was sufficient to induce higher sensitivity to AICAR, while the inactivation of *S6K2* had no effect (Figure 3D). Thus, the differential sensitivity to AMPK activation depends on S6K1 expression and has functional consequences on glucose homeostasis in the animal.

Energy Metabolism Is Altered by *S6K* Deletion

To gain further insights into the functional significance of AMPK activation at the cellular level, we evaluated mitochondrial enzyme activities in *S6K1;S6K2*$^{-/-}$ muscle cells. Mitochondria are the main site of substrate oxidation within the cell, and their biogenesis is upregulated by the AMPK pathway (Zong et al., 2002). The activity of two mitochondrial enzymes, citrate synthase and cytochrome *c* oxidase, was increased by 50%–70% in *S6K1;S6K2*$^{-/-}$ myotubes (Figures 4A and 4B), while the activity of the glycolytic enzyme hexokinase did not differ as compared to wild-type control (Figure 4C). Mitochondrial fatty acid β oxidation, a major target of AMPK regulation (Kahn et al., 2005), was also augmented in mutant muscle cell cultures, as measured by [^{3}H]palmitate oxidation (Figure 4D). Furthermore, these functional changes were accompanied

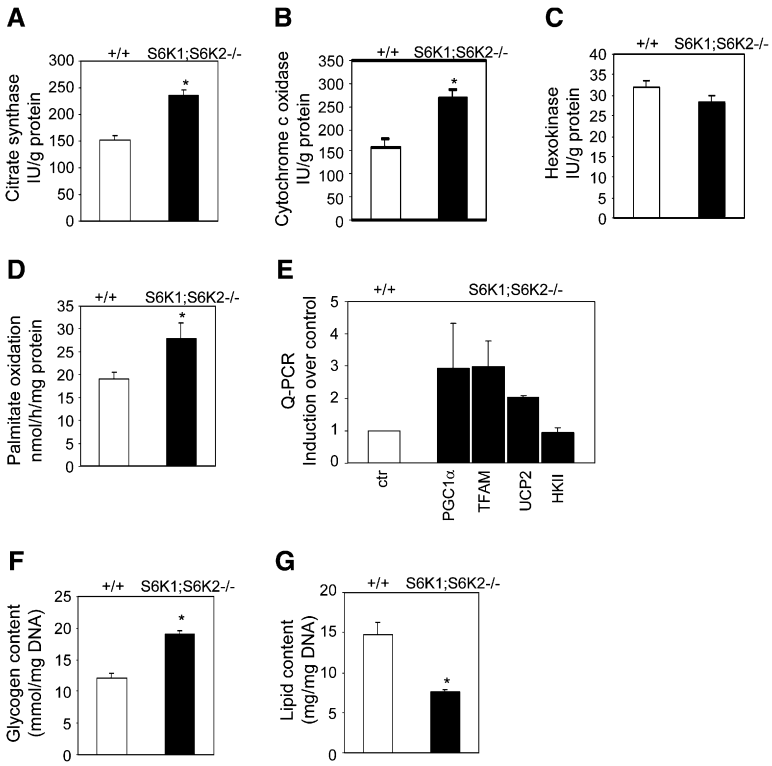

Figure 4. Increased Mitochondrial Mass and Activity in *S6K*-Deficient Muscle Fibers Is Accompanied by Lipid Content Depletion and Glycogen Sparing

(A–C) Assessment of citrate synthase, cytochrome *c* oxidase, and hexokinase was performed in cells at day 4 of differentiation.

(D) Fatty acid β-oxidation was measured in myoblast cells maintained in complete medium for 2 days. ($n \geq 3$ assays.) Independent cell cultures were obtained from at least three mice of the indicated genotype.

(E) Total RNA was isolated from muscle cells allowed to differentiate for 4 days in 2% horse serum. Gene expression levels were quantified by RT-qPCR. ($n \geq 3$ assays.) Independent cell cultures were obtained from at least two mice of the indicated genotype.

(F and G) Hindlimb muscles from 7–11 mice of the indicated genotype were pooled, and glycogen (F) and lipid (G) content was measured. n = 3 pools of the indicated genotype; *$p < 0.01$ versus wild-type genotype.

by the upregulation of mRNAs encoding the PPARγ transcriptional coactivator 1α (PGC-1α) and the mitochondrial transcription factor A (TFAM) (Figure 4E), two factors required for mitochondrial biogenesis (Wu et al., 1999), while hexokinase mRNA levels were unchanged. In addition, the expression of the uncoupling protein-2 (*UCP2*) gene, a PGC-1α target that may affect proton leak from mitochondria (Wu et al., 1999), was increased in mutant myotubes. As previously reported for *S6K1*$^{-/-}$ white adipose tissue and plantaris muscle (Um et al., 2004), we observed an increased mitochondrial mass by electron microscopy in cultured *S6K1;S6K2*$^{-/-}$ myotubes (data not shown). In conclusion, *S6K* deletion leads to a cell-autonomous upregulation of mitochondrial mass, activity, and β-oxidation.

To measure the regulation of mitochondrial substrate utilization by phosphate acceptors, we evaluated the ADP dependency of respiration rates in permeabilized fibers from gastrocnemius and soleus muscles. As expected, the utilization of glutamate and malate substrates was more pronounced in the oxidative slow-twitch soleus muscles as compared to the glycolytic fast-twitch gastrocnemius (Figure S3). In both muscle types, the respiration rate independent of ADP phosphorylation (V_0) was increased in *S6K1;S6K2*$^{-/-}$ fibers, suggesting a state of energy expenditure and increased basal metabolism. The maximal respiration rate in the presence of saturating ADP levels (V_{max}) was also increased in *S6K1;S6K2*$^{-/-}$ fibers. Therefore, the coupling ratio, as defined by the V_{max}/V_0 ratio (ACR), was not significantly different among the two genotypes and did not reveal uncoupling defects in permeabilized mutant fibers under controlled extramitochondrial medium and energy substrates.

The two major energy sources in skeletal muscles are glycogen and lipids. Since we observed increased fatty acid oxidation in *S6K*-deficient myotubes, we quantified the nature of energy stores in muscle. The glycogen amount was more abundant in *S6K1;S6K2*$^{-/-}$ gastrocnemius as compared to wild-type, while the total lipid content was reduced by half (Figures 4F and 4G). Thus, the *S6K* deletion promotes the sparing of glycogen accompanied by a shift toward mitochondrial fatty acid oxidation, possibly due to the concomitant increase in mitochondrial biogenesis and downregulation of ACC. These metabolic adaptations recapitulate a state of increased AMPK signaling, as observed in prolonged fasting or endurance exercise (Kahn et al., 2005).

AMPK Inhibition Rescues *S6K*$^{-/-}$ Cell Growth

To address whether the increased AMPK activity is implicated in the growth defect of *S6K*-deficient muscle cells, we overexpressed by adenovirus-mediated gene transfer a mutant form of *AMPKα2* carrying a K45R substitution. This kinase-dead mutant (*kd-AMPK*) induces the partial degradation of endogenous AMPKα subunits and acts as a dominant-inhibitory allele (Mu et al., 2001). A slower migrating AMPK immunoreactive band corresponding to the myc-tagged mutant was observed in *kd-AMPK*-expressing myotubes as compared to *GFP*-transduced control cells (Figure 2C). kd-AMPK decreased the expression of the endogenous AMPKα subunit, resulting in the

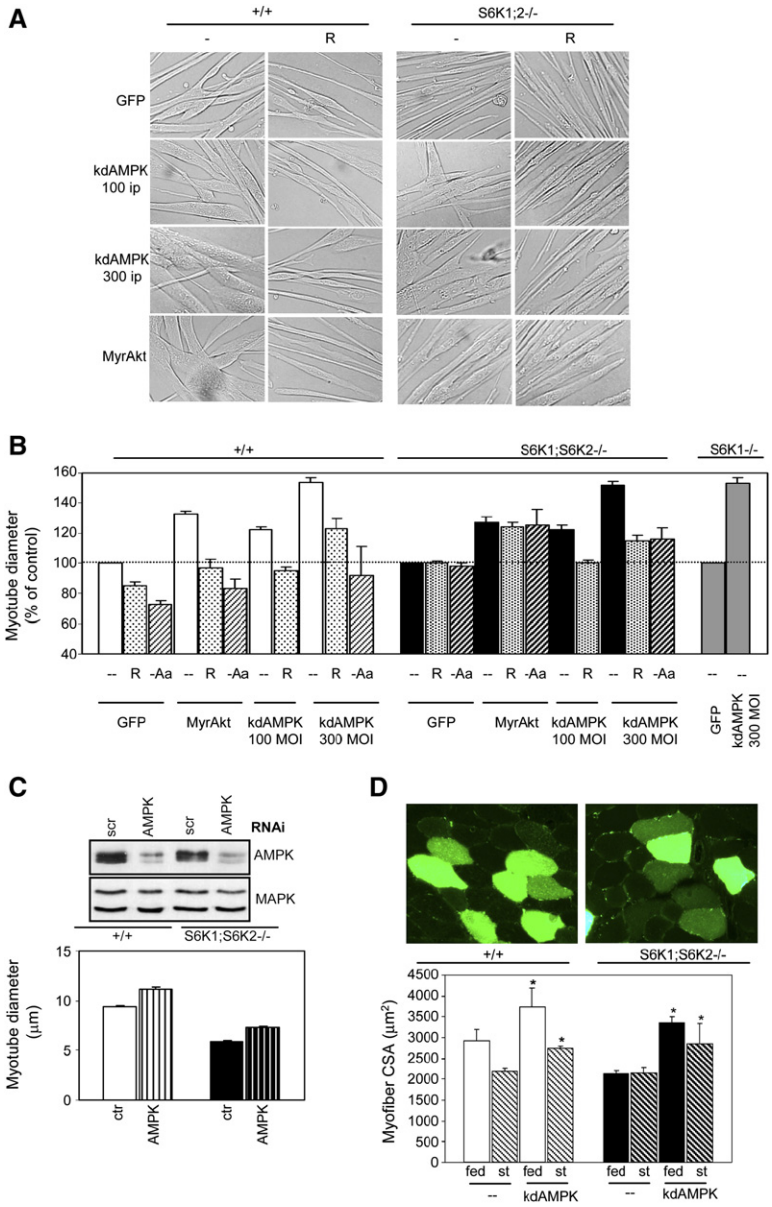

Figure 5. AMPK Inhibition Partially Rescues Cell Size

(A and B) Cells of the indicated genotype were allowed to differentiate for 2 days and were transduced with 150 moi *GFP*, 150 moi constitutively active Akt (*MyrAkt*), or *kd-AMPK* adenoviruses at the indicated moi. Where indicated, cells were then treated with 20 nM rapamycin (R) or cultured in amino acid-free medium (−Aa). After 2 days, myotube diameter was measured and expressed as percentage change over GFP-transduced cells of the appropriate genotype. Representative bright-field images are shown in (A). Data from two to five experiments are shown in histograms in (B).

(C) Immunoblot analysis of protein extracts from myotubes using the indicated antibodies. Cells were transfected with 20 nM control or *AMPK* siRNA at day 1 of differentiation and harvested 3 days later. The lower panel shows the average myotube diameter from two distinct experiments.

(D) Tibialis anterior muscles were coelectroporated with *kd-AMPK* and *GFP* cDNAs, the latter as a marker of transfection. Fiber cross-sectional area in transfected and untransfected fibers was measured. Representative bright-field images are shown in the upper panel. n = 2–6 muscles in histograms in lower panel; *p $\leq$ 0.05 versus untransfected fibers.

inhibition of ACC phosphorylation and the increase of total ACC expression. Conversely, kd-AMPK promoted mTOR signaling, as indicated by the increased phosphorylation of 4EBP-1 and S6K1. Next, the effect on myotube size was measured 48 hr after transduction. As previously reported (Ohanna et al., 2005), the size of *S6K*-deficient myotubes was smaller (6.2 ± 0.2 μm diameter for GFP-expressing *S6K1;S6K2*$^{-/-}$ muscle cells versus 8.9 ± 0.5 for wild-type cells) and was completely resistant to the inhibitory effects of rapamycin or amino acid starvation (Figures 5A and 5B), demonstrating that *S6K* inactivation mimics an atrophic status triggered by nutrient/mTOR depletion. The hypertrophic action of constitutively active Akt1 (MyrAkt) in wild-type cells was mediated by rapamycin-sensitive and -insensitive pathways, as previously observed (Rommel et al., 2001; Ohanna et al., 2005). Rapamycin treatment or amino acid deprivation had no effect on MyrAkt-induced cell growth in *S6K1;S6K2*$^{-/-}$ myotubes, indicating that the mTOR-independent branch is the only mechanism operating in these cells. *kd-AMPK* expression led to a dose-dependent growth of both wild-type and *S6K1;S6K2*$^{-/-}$ cells. The size of *S6K1*$^{-/-}$ cells was comparable to double mutants (Ohanna et al., 2005; Figure S2) and was also rescued by *kd-AMPK* expression (Figure 5B). In addition, an RNAi targeting both α1 and α2 catalytic subunits of AMPK reproduced the effect of *kd-AMPK* expression on cell size of wild-type and mutant *S6K* genotypes (Figure 5C). Taken together, these data demonstrate that AMPK activity contributes to the size control of muscle cells.

Strikingly, AMPK inhibition not only rescued the atrophy of *S6K1;S6K2*$^{-/-}$ cells but also conferred sensitivity to the activation of the nutrient/mTOR pathway, as rapamycin and amino acid starvation blunted growth of *kd-AMPK*-expressing *S6K1;S6K2*$^{-/-}$ cells (Figure 5B). The inhibition by rapamycin was approximately 70% at the *kd-AMPK* dose of 300 moi, suggesting that mTORC1-dependent and -independent pathways promote cell growth when *S6K* is deleted and AMPK is inhibited.

To extend our findings in vivo, we electroporated *kd-AMPK* and *GFP* cDNAs in the tibialis anterior muscles of wild-type and *S6K1;S6K2*$^{-/-}$ mice. Twelve days after electroporation, mice were either starved for 48 hr or allowed free access to food. As shown in Figure 5D, in wild-type mice, starvation reduced the cross-sectional area (CSA) of untransfected fibers by 25%, though the *S6K1;S6K2*$^{-/-}$ fiber size was completely resistant to food deprivation. Of note, the *kd-AMPK*-transfected fibers in wild-type and in *S6K1;S6K2*$^{-/-}$ muscles were 27% and 57% larger, respectively, as compared to untransfected fibers. In addition, their growth was dependent on food intake. In conclusion, we demonstrate that the energy stress triggered by *S6K1* deletion upregulates the AMPK pathway, which in turn switches on a starvation-like metabolic program and arrests growth. Inhibition of this AMPK-dependent response allows cell mass accumulation in response to nutrient availability.

DISCUSSION

The energy charge of the adenine nucleotide pool is the universal coupling agent of metabolism, providing the directionality toward the synthesis or the degradation of cellular constituents (Atkinson, 1970). Metazoans have developed a complex signal transduction network that coordinates the energy status of the cell with extracellular growth factors and nutrient availability to regulate growth rates. In this study, we show that the suppression of nutrient-activated mTOR/S6K1 signaling is sufficient to trigger an energy stress response that is coordinated by AMPK. This AMPK-dependent metabolic program blunts the growth responses to nutrient availability and thereby plays a central role in the atrophic phenotype of *S6K1*-deficient animals.

The crosstalk between S6K and AMPK is emerging as a powerful and highly regulated way to gauge cellular energy and nutrition content leading to changes in growth and metabolic rates. In skeletal muscles, the AMPK module predominates during low-calorie diet and endurance exercise, while the S6K module is turned on during high-calorie diet and resistance exercise (Atherton et al., 2005; Um et al., 2004). It was previously shown that AMPK downregulates mTOR/S6K signaling via TSC2 phosphorylation (Inoki et al., 2003). Here we provide evidence that the reverse regulation also takes place in the cell, as S6K signaling controls AMPK by affecting the AMP/ATP ratio (Figure 1 and Figure 2). This tight control probably serves the important function of enforcing the unidirectionality of metabolic sequences during a particular energy status and avoiding futile cycles in which synthesis and degradation are simultaneously turned on. Due to these counterregulatory mechanisms, *S6K* deletion leads to opposite traits as compared to the inhibition of AMPK signaling in skeletal muscles. The expression of a kinase-dead form of AMPK or the inactivation of the muscle-specific AMPKγ3 subunit causes a decrease in PGC-1α expression, a defect in mitochondrial biogenesis and in glycogen synthesis, and a slight increase in fiber size (Mu et al., 2001; Zong et al., 2002; Mu et al., 2003; Nilsson et al., 2006; Krawiec et al., 2007), while *S6K*$^{-/-}$ muscle fibers have small size (Figure 1 and Figure 5) and increased glycogen content, mitochondrial mass, and enzymatic activities that are accompanied by the upregulation of PGC-1α and TFAM (Figure 4). When the kinase-dead AMPK mutant is introduced in *S6K*-deficient muscle cells, the defect in cell growth is rescued (Figure 5), suggesting that the AMPK-dependent metabolic program is a downstream target of the S6K pathway and contributes to the phenotype of *S6K*-deficient muscles.

Of note, AMPK inhibition renders *S6K1;S6K2*$^{-/-}$ cell growth sensitive to nutrient availability and mTOR activity, suggesting that additional rapamycin-sensitive mTOR substrates regulate muscle growth when AMPK is inhibited (Figure 5). These may include the eIF4E-binding proteins that are hyperphosphorylated in cells expressing a dominant-inhibitory form of AMPK (Figure 2C). Additional molecular mechanisms that regulate protein synthesis and ribosome biogenesis downstream of mTOR and independent of S6K activity (Pende et al., 2004) are likely to participate in muscle growth when the inhibitory action of AMPK is relieved. Thus, we propose that S6K activity sensitizes skeletal muscle cells to growth factors and nutrients through AMPK regulation rather than directly affecting cell growth. Although no known physiological condition displays inactive S6K while mTORC1 is active, the genetic inactivation of *S6K* unveils this molecular mechanism that may become clinically relevant when selective S6K inhibitors are developed. Interestingly, environmental signals mainly affect growth of glycolytic muscle fibers while sparing oxidative fibers, as observed during cachexia- or malnutrition-induced atrophy (Mendell and Engel, 1971). Since *S6K*-deficient muscle cells display increased oxidative metabolism and resistance to nutrient levels, it is possible that the S6K-AMPK gauge determines muscle plasticity to environmental cues by altering the glycolytic-oxidative properties.

Our study sheds light on the S6K-dependent utilization of glucose and fatty acids, the two major energy sources in skeletal muscles. By a series of biochemical and gene expression analyses, we have established that *S6K*-deficient muscles preferentially use fatty acids rather than glucose, leading to a sharp difference in lipid and glycogen content as compared to wild-type (Figure 4). This response is typically observed in muscles after long-term starvation or endurance exercise (Jagoe et al., 2002), possibly involving AMPK-PGC-1α-mediated mechanisms (Atherton et al., 2005). How does the suppression of S6K1 signaling in skeletal muscle affect the energy charge

of the adenine nucleotide pool? One possibility is that specific energy substrates are limiting in *S6K*-deficient muscles in vivo, e.g., due to the suppression of specific uptake systems. Although an exhaustive list of uptake systems was not analyzed in this study, our data failed to uncover a defect in the uptake of glucose, system A substrates, or the complete amino acid mixture in isolated muscle (data not shown; Pende et al., 2000). To analyze the processes of intracellular nutrient utilization, we next evaluated mitochondrial respiration, the main energy-producing system. When the mitochondria from *S6K*-deficient muscle fibers were provided with glutamate and malate substrates in a controlled medium, no functional uncoupling of the respiratory chain was revealed (Figure S3). Since these studies were conducted in permeabilized fibers, we cannot rule out the possibility that specific energy substrates or decoupling agents are affecting oxidative phosphorylation in vivo. However, our data favor the possibility of an increased energy expenditure state that is triggered by *S6K* inactivation. Interestingly, a number of conditions appear to reproduce a similar metabolic program in skeletal muscle. Stimulation by adiponectin (Civitarese et al., 2006) or CNTF (Watt et al., 2006), sirtuin activation by resveratrol (Baur et al., 2006), and stearoyl-CoA desaturase deficiency (Dobrzyn et al., 2004) also alter the energy balance and activate AMPK, suggesting novel crosstalk between these factors and the mTOR/S6K signaling.

S6K1 is emerging as a key factor promoting cell mass accumulation in response to nutrition and downregulating insulin action in adipose tissue and skeletal muscles (Um et al., 2004; Ohanna et al., 2005). Consistent with this, S6K1 is hyperactive in animal models of obesity (Um et al., 2004). However, little is known about its mechanism of action. The phosphorylation of translation factors or IRS proteins has been put forward to explain S6K1 effects on growth or insulin sensitivity, though direct evidence is lacking. Our results indicate that the suppression of S6K1 activity simultaneously promotes AMPK and Akt signaling (Figure 2), thus ameliorating metformin and insulin action, which represent two major diabetes therapies. In conclusion, the control of energy charge and AMPK activity by S6K1 contributes to glucose homeostasis and muscle plasticity, providing a molecular mechanism that may represent an attractive target in metabolic syndromes.

EXPERIMENTAL PROCEDURES

Animals

Generation of *S6K*-deficient mice has been previously described (Shima et al., 1998; Pende et al., 2004). AICAR tolerance tests were performed in the morning by intraperitoneal injection of 0.15 g AICAR (Biomol) per kg body weight into overnight-fasted mice. Blood was collected from the tail vein at 0, 15, 30, 45, and 100 min after injection for determination of glucose levels by Glucotrend glucometer (Roche Diagnostics).

Cell Cultures

Primary muscle cell cultures were derived from gastrocnemius and tibialis anterior muscles of 4-week-old mice as described (Ohanna et al., 2005). Primary hepatocytes were prepared as described (Pende et al., 2004). To measure the effect of ectopic gene expression on size, myotubes at day 2 of differentiation were transduced by *kd-AMPK* (kindly provided by M.J. Birnbaum, University of Pennsylvania School of Medicine), *GFP*, or *MyrAkt* adenovirus at the indicated moi and incubated for 2 days in DMEM/Ham's F12 medium + 2% horse serum. When indicated, transduced cells were treated with 20 nM rapamycin or grown in amino acid-free DMEM + 2% dialyzed horse serum for 2 days. For RNA interference against S6K and AMPK, 21-nucleotide siRNA duplexes with two deoxythymidine bases as 3′ overhangs were synthesized corresponding to *S6K1/2* target sequence (5′-CTCAGTGA GAGTGCCAACCAA-3′), *AMPKα1/α2* target sequence (5′-AAGAGA AGCAGAAGCACGACG-3′), and control (5′-AAGCCGGTATGCCGGT TAAGT-3′). Myotubes at day 1 of differentiation were transfected with 20 nM siRNA using HiPerFect (QIAGEN). Cells were harvested 3 days after transfection. Bright-field images were taken of live cells and analyzed using Lucia archive software. The diameter of at least 400 myotubes was measured in a region where myonuclei were absent and diameter was constant.

Immunoblotting

For immunoblot analysis, cells were washed twice with cold phosphate-buffered saline (PBS), scraped off of the culture dish in lysis buffer B (50 mM Tris [pH 8.0], 1% NP-40, 120 mM NaCl, 20 mM NaF, 1 mM benzamidine, 1 mM EDTA, 1 mM EGTA, 15 mM sodium pyrophosphate, 1 mM PMSF, 2 mM sodium orthovanadate, 2 μg/ml leupeptin, 5 μg/ml aprotinin, 1 μg/ml pepstatin A), and sonicated for 30 s. Adipose tissue was lysed in 20 mM Tris-HCl (pH 8.0), 5% glycerol, 138 mM NaCl, 2.7 mM KCl, 1% NP-40, 20 mM NaF, 5 mM EDTA, 1 mM sodium orthovanadate, 5 μg/ml leupeptin, 1 μg/ml pepstatin, 1 mM DTT. To remove cell debris, homogenates were spun at 8000 × g for 10 min at 4°C. Protein extract was resolved by SDS-PAGE before transfer onto nitrocellulose membrane and incubation with the following primary antibodies: anti-phospho-Thr389 S6K1, anti-phospho-Thr172 AMPKα, anti-AMPKα, anti-phospho-Ser79 ACC, anti-ACC, anti-phospho-Ser473 Akt, anti-Akt, anti-4EBP-1, anti-phospho-Ser65 4EBP-1 (Cell Signaling), monoclonal anti-S6K2 (kindly provided by G. Thomas, University of Cincinnati), anti-α-tubulin (TU-02, Santa Cruz), anti-MAPK (Upstate Biotechnology). To estimate the levels of phosphorylation of AMPK, Akt, and S6K reported relative to total protein or tubulin, densitometry was performed using ImageJ software (http://rsb.info.nih.gov/ij/).

Quantitative RT-PCR

Total RNA was prepared using TRIzol reagent according to the manufacturer's protocol (Life Technologies), and single-strand cDNA was synthesized from 400 ng of total RNA with random hexamer primers and SuperScript II (Invitrogen). Real-time quantitative PCR (RT-qPCR) was performed using a LightCycler instrument (Roche) according to the manufacturer's instructions using a SYBR Green I kit (QIAGEN). Briefly, the final volume of 20 μl contained 16 ng of reverse-transcribed total RNA, 1 nM of primer mix, 10 μl of 2× SYBR Green PCR mix. Reactions were carried out in capillaries (Roche) with 40 cycles. We determined the relative amounts of the mRNAs studied by means of the second-derivative maximum method, with LightCycler analysis software version 3.5 and β-actin as the invariant control for all studies. RT-qPCR primers were designed using sequences available in PrimerBank and spanned an intron/exon boundary. The murine primer sequences used were peroxisome proliferator-activated receptor α (*PGC-1α*) sense 5′-GGAATGCACCGTAAATCT GC-3′, antisense 5′-TTCTCAAGAGCAGCGAAAGC-3′; hexokinase II (*HKII*) sense 5′-TGATCGCCTGCTTATTCACGG-3′, antisense 5′-AAC CGCCTAGAAATCTCCAGA-3′; β-*actin* sense 5′-CTGGCTCCTAG CACCAAGAT-3′, antisense 5′-GGTGGACAGTGAGGCCAGGAT-3′; mitochondrial transcription factor A (*TFAM*) sense 5′-GGAATGT GGAGCGTGCTAAAA-3′, antisense 5′-ACAAGACTGATAGACGAGG GG-3′; *UCP2* sense 5′-ACTTTCCCTCTGGATACCGC-3′, antisense 5′-ACGGAGGCAAAGCTCATCTG-3′. The results of RT-qPCR are

given in arbitrary units and expressed as fold changes in mRNA levels relative to wild-type controls.

Biochemical Studies

For enzymatic activities, myotube cell cultures were washed and quickly frozen in liquid nitrogen. Cells were scraped off of the culture dish and homogenized into ice-cold buffer containing 5 mM HEPES, 1 mM EGTA, 5 mM $MgCl_2$, 1 mM dithiothreitol, 0.1% Triton X-100 (pH 8.7) and incubated for 60 min at 0°C to ensure complete enzyme extraction. Citrate synthase, hexokinase, and cytochrome *c* oxidase were assessed by standard spectrophotometric methods (Srere, 1969; Bergmeyer et al., 1974).

For adenine nucleotides and PCr assays, mice were anesthetized by intraperitoneal injection of 5% Rompun and 20% Imalgene 1000. Liver and hindlimb muscles comprising gastrocnemius, soleus, and plantaris were quickly removed using cold forceps and snap frozen in liquid nitrogen. Metabolites were extracted with perchloric acid, and ATP, AMP, and PCr were measured in neutralized supernatant by coupled enzyme assays (Bergmeyer, 1974).

For adenine nucleotide measurement in cell cultures, 6 cm plates with myotubes at day 4 of differentiation were washed twice with PBS and scraped in perchloric acid to a final concentration of 5% (wt/vol). Acid-insoluble material was removed by centrifugation, and perchloric acid was extracted from the supernatant by three washes with 10% excess (by volume) of a 1:1 mixture of tri-*n*-octylamine and 1,1,2-trichlorotrifluoroethane. Nucleotides were separated by ion-exchange chromatography on a Mono Q PC1.6/5 column run on a SMART System (Amersham Biosciences) as described elsewhere (Fryer et al., 2002). Nucleotides were detected by their absorbance at 254 nm and compared with the elution position of standards. Areas under the AMP and ATP peaks were quantified by integration using SMART System software and used to calculate the AMP/ATP ratios.

For lipid and glycogen content, frozen tissue samples were ground in liquid nitrogen, yielding a homogeneous tissue powder that was divided in two aliquots. One aliquot was dried by lyophilization. The lipids of freeze-dried powders were extracted by petrol ether. Lipid-free powder was dried and used for determination of DNA contents by a diphenylamine assay (Forsberg et al., 1991). The other aliquot was used for enzymatic analysis of glycogen after perchloric acid extraction (Bergmeyer, 1974).

The respiratory parameters of the total mitochondrial population were studied in situ in saponin-skinned fibers using a method described earlier (Veksler et al., 1995). Briefly, respiratory rates were determined using a Clark electrode in an oxygraphic cell at 22°C with continuous stirring. Thin muscle fibers were isolated in skinning (S) solution containing (in mmol/l) 2.77 CaK_2 EGTA, 7.23 K_2 EGTA, 6.56 $MgCl_2$, 5.7 Na_2 ATP, 15 PCr, 20 taurine, 0.5 DTT, 50 K methanesulfonate, 20 imidazole (pH 7.1) and incubated for 30 min in S solution with 50 μg/ml saponin. Permeabilized fibers were transferred to respiration (R) solution (composition as S solution, but containing 3 mmol/l K_2HPO_4 instead of PCr and ATP) for 10 min to wash out adenine nucleotides and PCr. All steps were carried out at 4°C with continuous stirring. Respiration rates of 10–15 mg of skinned fibers were measured at 22°C in 3 ml of R solution containing 2 mg/ml bovine serum albumin with 5 mM glutamate and 2 mM malate as substrates. Sensitivity to ADP was determined by measuring respiration rates with increasing levels of ADP. ADP-stimulated respiration (V_{ADP}) above basal oxygen consumption (V_0) was plotted as a function of [ADP]. V_{ADP} was calculated using a nonlinear fitting of the Michaelis-Menten equation. Maximal respiration rate (V_{max}) was $V_{ADP} + V_0$. Acceptor control ratio (ACR) was calculated as V_{max}/V_0. After the experiment, fiber bundles were dried and weighed. Rates of respiration are given in μmol O_2/min/g dry weight.

NMR Measurements

^{31}P NMR of mouse gastrocnemius was carried out using a Bruker Biospec 47/50 operating at 4.7 T equipped with a 12 cm gradient insert. For this purpose, a 1.5 cm diameter Helmholtz transmit/receive radiofrequency (RF) coil tuned at 81 MHz was designed in order to ensure a correct localization of the NMR signal. Mice were anesthetized with isoflurane (1.5% in air) and positioned prone in the magnet. The RF coil was placed around both mouse hindlimbs. Proton shimming was performed in order to reach a linewidth at half-height of typically 40 Hz for the water resonance. ^{31}P NMR spectra (100 μs RF pulse, 2.8 s interpulse delay, 2048 data points, 1024 free induction decays, 15 Hz Lorentzian filter before Fourier transformation) were acquired within 47 min. Spectra were then analyzed as a sum of Lorentzian-Gaussian lineshaped resonances in order to determine the areas of the nucleoside triphosphate (NTP) and the PCr resonances. The PCr, Pi, and β-ATP peak areas were calculated and converted to concentrations with [ATP] = 8.2 mmol/l (Kushmerick et al., 1993). Free energy of ATP hydrolysis (ΔGp) was calculated as ΔG^0 + RT ln([ADP][Pi][H+]/[ATP]), where ΔG^0 = 9.742 kJ/mol, at 37°C, derived from Gibbs free energy of hydrolysis under standard conditions at pH = 7.

Palmitate Oxidation

Fatty acid oxidation was measured by quantifying the production of ^3H_2O from [9,10-^{3}H]palmitate. The satellite cells were trypsinized, counted, plated at 4 × 10^4 cells per well in 24-well gelatin-coated culture plates, and allowed to grow for 2 days. Tritiated water release experiments were performed in quadruplicate. Cultured muscle cells were washed three times with Dulbecco's PBS. Then, 200 μl of [9,10(n)-^{3}H]palmitic acid (60 Ci/mmol, NEN) bound to fatty-acid-free albumin (final concentration 125 μM) containing 1 mM carnitine was added per well. After 2 hr incubation at 37°C, the mixture was removed and added to a tube containing 200 μl of cold 10% trichloroacetic acid (TCA). The tubes were centrifuged for 10 min at 2200 × g at 4°C, and aliquots of supernatants (350 μl) were removed, mixed with 55 μl of 6 M NaOH, and applied to ion-exchange resin. The columns were washed twice with 750 μl of water, and the eluates were counted. Cell protein content was determined by the Lowry method. Palmitate oxidation rates were expressed as nmol of [^{3}H]palmitate oxidized per hr per mg of cell protein (nmol [^{3}H]FA/hr/mg protein).

In Vivo Transfection Experiments and Fiber Size Measurements

Experiments were performed in 3-month-old mice. In vivo transfection of tibialis anterior muscles was performed by intramuscular injection of plasmids carrying myc-tagged *kd-AMPK* and *GFP* cDNAs followed by electroporation as described (Sandri et al., 2004). Muscles were removed at 14 days after transfection and frozen in liquid nitrogen for fiber size measurements. Mice were either randomly fed or fasted 48 hr before sacrifice. Muscle fiber size was measured in fibers transfected with the *kd-AMPK* mutant using GFP staining as a probe and in an equal number of untransfected fibers from the same muscle. Fiber cross-sectional areas were measured using Image software (Scion Corporation).

Supplemental Data

Supplemental Data include three figures and can be found with this article online at http://www.cellmetabolism.org/cgi/content/full/5/6/476/DC1/.

ACKNOWLEDGMENTS

We thank the Novartis Foundation and the G. Thomas laboratory for the use of *S6K* mutant mice. We are grateful to F. Bouillaud and G. Thomas for reading the manuscript and helpful discussions and to the members of INSERM U845 for support. We thank Frimorfo Inc., Philippe Mateo, and D. Fortin for skillful technical assistance. This work was supported by grants from the INSERM Avenir program (to M.P.), the Fondation de la Recherche Médicale, the Fondation Schlumberger pour l'Education et la Recherche, the Association Française contre les Myopathies (to A. Sotiropoulos and M.P.), the Association Nationale de la Recherche (to B.V. and M.P.), and Telethon (to M.S.). S.A. is a recipient of a stipend from Region Ile-de-France and

Association de Recherche sur le Cancer. R.V.-C. is a Centre National de la Recherche Scientifique employee.

Received: October 26, 2006
Revised: March 20, 2007
Accepted: May 11, 2007
Published: June 5, 2007

REFERENCES

Atherton, P.J., Babraj, J., Smith, K., Singh, J., Rennie, M.J., and Wackerhage, H. (2005). Selective activation of AMPK-PGC-1alpha or PKB-TSC2-mTOR signaling can explain specific adaptive responses to endurance or resistance training-like electrical muscle stimulation. FASEB J. *19*, 786–788.

Atkinson, D.E. (1970). Adenine nucleotides as universal stoichiometric metabolic coupling agents. Adv. Enzyme Regul. *9*, 207–219.

Baur, J.A., Pearson, K.J., Price, N.L., Jamieson, H.A., Lerin, C., Kalra, A., Prabhu, V.V., Allard, J.S., Lopez-Lluch, G., Lewis, K., et al. (2006). Resveratrol improves health and survival of mice on a high-calorie diet. Nature *444*, 337–342.

Bergmeyer, H.U. (1974). Metabolites: nucleic acids, purines, pyrimidines, nucleosides, coenzymes. In Methods of Enzymatic Analysis, H.U. Bergmeyer, ed. (Weinheim, Germany: Verlag Chemie), pp. 1836–1839.

Bergmeyer, H.U., Gawehn, K., and Grassl, M. (1974). Hexokinase. In Methods of Enzymatic Analysis, H.U. Bergmeyer, ed. (Weinheim, Germany: Verlag Chemie), pp. 473–474.

Civitarese, A.E., Ukropcova, B., Carling, S., Hulver, M., DeFronzo, R.A., Mandarino, L., Ravussin, E., and Smith, S.R. (2006). Role of adiponectin in human skeletal muscle bioenergetics. Cell Metab. *4*, 75–87.

Dennis, P.B., Jaeschke, A., Saitoh, M., Fowler, B., Kozma, S.C., and Thomas, G. (2001). Mammalian TOR: a homeostatic ATP sensor. Science *294*, 1102–1105.

Dobrzyn, P., Dobrzyn, A., Miyazaki, M., Cohen, P., Asilmaz, E., Hardie, D.G., Friedman, J.M., and Ntambi, J.M. (2004). Stearoyl-CoA desaturase 1 deficiency increases fatty acid oxidation by activating AMP-activated protein kinase in liver. Proc. Natl. Acad. Sci. USA *101*, 6409–6414.

Edinger, A.L., and Thompson, C.B. (2002). Akt maintains cell size and survival by increasing mTOR-dependent nutrient uptake. Mol. Biol. Cell *13*, 2276–2288.

Foretz, M., Ancellin, N., Andreelli, F., Saintillan, Y., Grondin, P., Kahn, A., Thorens, B., Vaulont, S., and Viollet, B. (2005). Short-term overexpression of a constitutively active form of AMP-activated protein kinase in the liver leads to mild hypoglycemia and fatty liver. Diabetes *54*, 1331–1339.

Forsberg, A.M., Nilsson, E., Werneman, J., Bergstrom, J., and Hultman, E. (1991). Muscle composition in relation to age and sex. Clin. Sci. (Lond.) *81*, 249–256.

Fryer, L.G., Parbu-Patel, A., and Carling, D. (2002). Protein kinase inhibitors block the stimulation of the AMP-activated protein kinase by 5-amino-4-imidazolecarboxamide riboside. FEBS Lett. *531*, 189–192.

Hahn-Windgassen, A., Nogueira, V., Chen, C.C., Skeen, J.E., Sonenberg, N., and Hay, N. (2005). Akt activates the mammalian target of rapamycin by regulating cellular ATP level and AMPK activity. J. Biol. Chem. *280*, 32081–32089.

Hammerman, P.S., Fox, C.J., and Thompson, C.B. (2004). Beginnings of a signal-transduction pathway for bioenergetic control of cell survival. Trends Biochem. Sci. *29*, 586–592.

Holz, M.K., Ballif, B.A., Gygi, S.P., and Blenis, J. (2005). mTOR and S6K1 mediate assembly of the translation preinitiation complex through dynamic protein interchange and ordered phosphorylation events. Cell *123*, 569–580.

Inoki, K., Zhu, T., and Guan, K.L. (2003). TSC2 mediates cellular energy response to control cell growth and survival. Cell *115*, 577–590.

Jagoe, R.T., Lecker, S.H., Gomes, M., and Goldberg, A.L. (2002). Patterns of gene expression in atrophying skeletal muscles: response to food deprivation. FASEB J. *16*, 1697–1712.

Kahn, B.B., Alquier, T., Carling, D., and Hardie, D.G. (2005). AMP-activated protein kinase: ancient energy gauge provides clues to modern understanding of metabolism. Cell Metab. *1*, 15–25.

Krause, U., Bertrand, L., and Hue, L. (2002). Control of p70 ribosomal protein S6 kinase and acetyl-CoA carboxylase by AMP-activated protein kinase and protein phosphatases in isolated hepatocytes. Eur. J. Biochem. *269*, 3751–3759.

Krawiec, B.J., Nystrom, G.J., Frost, R.A., Jefferson, L.S., and Lang, C.H. (2007). AMP-activated protein kinase agonists increase mRNA content of the muscle-specific ubiquitin ligases MAFbx and MuRF1 in C2C12 cells. Am. J. Physiol. Endocrinol. Metab. Published online January 30, 2007. 10.1152/ajpendo.00622.2006.

Kushmerick, M.J., Moerland, T.S., and Wiseman, R.W. (1993). Two classes of mammalian skeletal muscle fibers distinguished by metabolite content. Adv. Exp. Med. Biol. *332*, 749–760.

Majewski, N., Nogueira, V., Bhaskar, P., Coy, P.E., Skeen, J.E., Gottlob, K., Chandel, N.S., Thompson, C.B., Robey, R.B., and Hay, N. (2004). Hexokinase-mitochondria interaction mediated by Akt is required to inhibit apoptosis in the presence or absence of Bax and Bak. Mol. Cell *16*, 819–830.

Mendell, J.R., and Engel, W.K. (1971). The fine structure of type II muscle fiber atrophy. Neurology *21*, 358–365.

Montagne, J., Stewart, M.J., Stocker, H., Hafen, E., Kozma, S.C., and Thomas, G. (1999). Drosophila S6 kinase: a regulator of cell size. Science *285*, 2126–2129.

Mu, J., Brozinick, J.T., Jr., Valladares, O., Bucan, M., and Birnbaum, M.J. (2001). A role for AMP-activated protein kinase in contraction- and hypoxia-regulated glucose transport in skeletal muscle. Mol. Cell *7*, 1085–1094.

Mu, J., Barton, E.R., and Birnbaum, M.J. (2003). Selective suppression of AMP-activated protein kinase in skeletal muscle: update on 'lazy mice.' Biochem. Soc. Trans. *31*, 236–241.

Nilsson, E.C., Long, Y.C., Martinsson, S., Glund, S., Garcia-Roves, P., Svensson, L.T., Andersson, L., Zierath, J.R., and Mahlapuu, M. (2006). Opposite transcriptional regulation in skeletal muscle of AMP-activated protein kinase gamma3 R225Q transgenic versus knock-out mice. J. Biol. Chem. *281*, 7244–7252.

Nobukuni, T., Joaquin, M., Roccio, M., Dann, S.G., Kim, S.Y., Gulati, P., Byfield, M.P., Backer, J.M., Natt, F., Bos, J.L., et al. (2005). Amino acids mediate mTOR/raptor signaling through activation of class 3 phosphatidylinositol 3OH-kinase. Proc. Natl. Acad. Sci. USA *102*, 14238–14243.

Ohanna, M., Sobering, A.K., Lapointe, T., Lorenzo, L., Praud, C., Petroulakis, E., Sonenberg, N., Kelly, P.A., Sotiropoulos, A., and Pende, M. (2005). Atrophy of S6K1(−/−) skeletal muscle cells reveals distinct mTOR effectors for cell cycle and size control. Nat. Cell Biol. *7*, 286–294.

Pende, M., Kozma, S.C., Jaquet, M., Oorschot, V., Burcelin, R., March-and-Brustel, Y., Klumperman, J., Thorens, B., and Thomas, G. (2000). Hypoinsulinaemia, glucose intolerance and diminished beta-cell size in S6K1-deficient mice. Nature *408*, 994–997.

Pende, M., Um, S.H., Mieulet, V., Sticker, M., Goss, V.L., Mestan, J., Mueller, M., Fumagalli, S., Kozma, S.C., and Thomas, G. (2004). S6K1(−/−)/S6K2(−/−) mice exhibit perinatal lethality and rapamycin-sensitive 5′-terminal oligopyrimidine mRNA translation and reveal a mitogen-activated protein kinase-dependent S6 kinase pathway. Mol. Cell. Biol. *24*, 3112–3124.

Rommel, C., Bodine, S.C., Clarke, B.A., Rossman, R., Nunez, L., Stitt, T.N., Yancopoulos, G.D., and Glass, D.J. (2001). Mediation of IGF-1-induced

skeletal myotube hypertrophy by PI(3)K/Akt/mTOR and PI(3)K/Akt/GSK3 pathways. Nat. Cell Biol. *3*, 1009–1013.

Sandri, M., Sandri, C., Gilbert, A., Skurk, C., Calabria, E., Picard, A., Walsh, K., Schiaffino, S., Lecker, S.H., and Goldberg, A.L. (2004). Foxo transcription factors induce the atrophy-related ubiquitin ligase atrogin-1 and cause skeletal muscle atrophy. Cell *117*, 399–412.

Sarbassov, D.D., Ali, S.M., and Sabatini, D.M. (2005). Growing roles for the mTOR pathway. Curr. Opin. Cell Biol. *17*, 596–603.

Sarbassov, D.D., Ali, S.M., Sengupta, S., Sheen, J.H., Hsu, P.P., Bagley, A.F., Markhard, A.L., and Sabatini, D.M. (2006). Prolonged rapamycin treatment inhibits mTORC2 assembly and Akt/PKB. Mol. Cell *22*, 159–168.

Shima, H., Pende, M., Chen, Y., Fumagalli, S., Thomas, G., and Kozma, S.C. (1998). Disruption of the p70(s6k)/p85(s6k) gene reveals a small mouse phenotype and a new functional S6 kinase. EMBO J. *17*, 6649–6659.

Srere, P.A. (1969). Citrate synthase. In Methods in Enzymology, S.P. Colowick and N.O.P. Kaplan, eds. (New York: Academic Press), pp. 3–11.

Um, S.H., Frigerio, F., Watanabe, M., Picard, F., Joaquin, M., Sticker, M., Fumagalli, S., Allegrini, P.R., Kozma, S.C., Auwerx, J., and Thomas, G. (2004). Absence of S6K1 protects against age- and diet-induced obesity while enhancing insulin sensitivity. Nature *431*, 200–205.

Um, S.H., D'Alessio, D., and Thomas, G. (2006). Nutrient overload, insulin resistance, and ribosomal protein S6 kinase 1, S6K1. Cell Metab. *3*, 393–402.

Veksler, V.I., Kuznetsov, A.V., Anflous, K., Mateo, P., van Deursen, J., Wieringa, B., and Ventura-Clapier, R. (1995). Muscle creatine kinase-deficient mice. II. Cardiac and skeletal muscles exhibit tissue-specific adaptation of the mitochondrial function. J. Biol. Chem. *270*, 19921–19929.

Watt, M.J., Dzamko, N., Thomas, W.G., Rose-John, S., Ernst, M., Carling, D., Kemp, B.E., Febbraio, M.A., and Steinberg, G.R. (2006). CNTF reverses obesity-induced insulin resistance by activating skeletal muscle AMPK. Nat. Med. *12*, 541–548.

Wu, Z., Puigserver, P., Andersson, U., Zhang, C., Adelmant, G., Mootha, V., Troy, A., Cinti, S., Lowell, B., Scarpulla, R.C., and Spiegelman, B.M. (1999). Mechanisms controlling mitochondrial biogenesis and respiration through the thermogenic coactivator PGC-1. Cell *98*, 115–124.

Zong, H., Ren, J.M., Young, L.H., Pypaert, M., Mu, J., Birnbaum, M.J., and Shulman, G.I. (2002). AMP kinase is required for mitochondrial biogenesis in skeletal muscle in response to chronic energy deprivation. Proc. Natl. Acad. Sci. USA *99*, 15983–15987.